JOURNAL OF APPLIED ELECTROCHEMISTRY 22 (1992) 835–842

Oxygen as a tracer for measurements of steady and turbulent flows

C. DESLOUIS, O. GIL, B. TRIBOLLET, G. VLACHOS

UPR 15 du CNRS "Physique des Liquides et Electrochimie" Université P. et M. Curie, 4 Place Jussieu 75252 Paris Cedex 05, France

B. ROBERTSON

Biotechnology Division, National Institute of Standards and Technology, Gaithersburg, MA 20899, U.S.A.

Received 15 March 1991; revised 25 November 1991

The reduction of dissolved oxygen has been studied over a wide conductivity range for use in steady or nonsteady hydrodynamic measurements. Mass transfer fluctuations can be analysed statistically to obtain the power spectra of hydrodynamic fluctuations. This requires a consideration of the proton reduction, which prevents diffusion from limiting the current. The transfer function for deducing the hydrodynamic spectra from mass transfer spectra includes not only transport effects but also kinetic effects which account for the finite rate of the reaction. The experimental study was performed using electrohydrodynamic (EHD) impedance.

1. Introduction

The polarographic method with microelectrodes has attracted great interest over the past twenty years since it provides a means of investigating flow properties or mass transport conditions closer to a wall than any other technique. For example, the steady-state fluid velocity gradient at the wall $\bar{\alpha}$ is related to the limiting diffusion current i_l by the Lévêque equation [1]

$$i_l \propto \bar{\alpha}^{1/3} \quad (1)$$

This relation is also valid in pulsed flow when applied to time dependent quantities in quasi steady-state conditions [2]. More recently, it has been shown that the spectral analysis of current fluctuations $i(t)$ yields the power spectral density W_i which is linked to the power spectral density of velocity gradient fluctuations W_α by [3, 4]

$$W_i = |H(\omega)|^2 W_\alpha \quad (2)$$

Here $H(\omega)$ is a transfer function, which depends on frequency $\omega/2\pi$ and which will be defined later.

The technique has been limited to laboratory studies because of the previous need to add an ionic tracer having a redox reaction of high standard rate and a supporting electrolyte in excess. For example, measurements of fluid flow in a marine environment with open systems, drainage of fresh water down a basin, study of thin liquid films in civil engineering and architecture [5] (e.g. entry of rain under combined influences of wind and gravity) have been beyond the capabilities of the technique. In addition, chemical or biochemical compatibility with the investigated medium must be ensured. Mass transport properties have been analysed for example in blood [6] with ferricinium chloroferrate (oxidizing ferrocene by ferric chloride) [7] as a tracer, and the diffusivity and the rheology of the medium have been investigated. The evolution of a fermentation process has also been studied by the polarographic method using platinum microelectrodes [8].

Oxygen is often already present in the fluids whose flow is to be studied. Most previous polarographic studies of oxygen were concerned with kinetics or the determination of the oxygen content in seas, natural waters or biological media. (For instance, the review by Hoare [9].) Only a few authors have tackled the problem of using oxygen in convective mass transport measurements in turbulence studies. (For example, Cornet *et al.* [10].) Those results are relevant to the marine environment since the experiments were conducted in 0.5 M NaCl solutions, which approaches sea water conditions.

In this work oxygen reduction was studied under steady flow conditions or under periodic flow conditions with a modulated rotating disc electrode (RDE) [11] over a wide range of NaCl concentrations. From this analysis, the diffusivity and the solubility of oxygen were measured, and the transfer function $H(\omega)$ of Equation 2, corresponding to a microelectrode, was deduced from that measured with the RDE and by considering the kinetic parameters of the reaction.

2. Experimental conditions

Solutions were prepared by adding NaCl pro-analysis reagent to bidistilled water maintained at 25 ± 0.1° C and in contact with air.

The effect of the metal is of some importance and has been reviewed in [9] for noble (inactive) or active metals. Only noble metals can be used as probes. In

0021-891X/92

preliminary experiments, platinum has showed some irreproducibility from day to day and also some tendency to increasing inactivity which may be due to significant absorption of oxygen and hydrogen by the crystal lattice. On the other hand, gold does not present those drawbacks, or at least does so but to a much lesser degree; and it also has a larger overpotential for hydrogen evolution than platinum. Another advantage is that gold is currently used in electroless deposits for preparing integrated circuits by the photolithography technique, which has been proposed recently for making microelectrodes of very small and precise dimensions as probes for hydrodynamic studies [12].

The rotating disc electrode (RDE) was the end of a gold rod (diam. 3 mm), the cylindrical side of which was protected from the solution by polyethylene shrink tubing. Prior to the experimental run the electrode was polished with emery paper (grade 1200) then polished with alumina powder (0.3 μm), carefully rinsed with distilled water in an ultra sonic bath and dried in warm air.

A rotating disc system (CNRS/AE patent no. 87.5503.00) was used, in which the angular speed was modulated sinusoidally so that its instantaneous value is

$$\Omega(t) = \bar{\Omega} + \mathrm{Re}\,(\tilde{\Omega} \exp j\omega t), \qquad (3)$$

where Re means the real part of a complex quantity. The experimental modulation frequency $\omega/2\pi$ ranged between 0 and 100 Hz with a modulation ratio $\tilde{\Omega}/\bar{\Omega}$ typically of 10% to ensure linearity. Modulation was supplied to the servo system controlling the angular velocity of the disc from the generator output of a Schlumberger 1250 frequency response analyser (FRA) and used to determine the electrohydrodynamical impedance (EHD) [11] in order to use the oxygen reduction for measurements of turbulence at the wall.

For greater accuracy, both current and velocity signals were filtered before input to the FRA as shown in the schematic diagram of the experimental setup in Fig. 1. Measurements were performed both with and without automatic compensation of the ohmic drop.

3. Results

3.1. *Steady-state measurements*

Current–potential curves for NaCl concentrations ranging from 0.5 M to 0.0033 M are presented in Fig. 2 with the ohmic drop subtracted out. The higher concentration data have larger currents and less defined diffusion plateaux with less cathodic hydrogen evolution overpotential.

Analysing the plateau current i_l against Ω requires selecting a potential common to all concentrations for which the oxygen reduction current is mass-transport limited. However, the proton reduction current which is insensitive to the rotation rate of the disc electrode, is superposed. Thus,

$$i = i_{H_2} + i_{lO_2}. \qquad (4)$$

Since i_{lO_2} is proportional to $\Omega^{1/2}$, the i against $\Omega^{1/2}$ plots, displayed in Fig. 3 are straight lines crossing the ordinate axis at the positive value i_{H_2}. As seen in the current–potential curves of Fig. 2, the component i_{H_2} for a given potential varies with the NaCl concentration. With i_{H_2} eliminated, the different straight lines follow the Levich equation [13]:

$$i_{lO_2} = 0.62nc_\infty FD^{2/3}\nu^{-1/6}\Omega^{1/2}\pi R^2 \qquad (5)$$

The lines are not parallel because the slope depends on the product $c_\infty D^{2/3}$. Since the viscosity, ν, depends weakly on the salt concentration and is only raised to the power $-1/6$, it has only a small relative effect.

At a potential of -1 V/SCE on gold, where the limiting current measurements were done, the oxygen reduction reaction is known to proceed in two steps, which, at neutral pH, are

$$\begin{cases} O_2 + 2e^- + 2H_2O \rightleftharpoons H_2O_2 + 2OH^- \\ H_2O_2 + 2e^- \rightleftharpoons 2OH^- \end{cases} \qquad (6)$$

The two steps are fast processes so that the overall reaction appears as a fast transfer of four electrons. Thus, all the factors on the right of Equation 5 are known *a priori* except c_∞ and $D^{2/3}$, so the product $c_\infty D^{2/3}$ can be determined by measuring the slope of the lines in Fig. 2.

The solubility of oxygen, c_∞, depends significantly on temperature, and on the kind and concentration of ions present in the solution. Oxygen diffusivity generally is around 2×10^{-5} cm^2 s^{-1} measured by several different techniques [14]. In this work the oxygen diffusivity has been determined by electrohydrodynamic impedance measurements and used to measure the solubility.

3.2. *EHD impedance measurements*

EHD impedance measurements were carried out at the same potential (i.e. -1 V/SCE) as that used for the plateau current determination. The time-dependent response of the current to a velocity modulation, such as in Equation 3, is $i(t) = \bar{i} + \mathrm{Re}\,(\tilde{i} \exp j\omega t)$ where $\tilde{i}$ is a complex quantity. The frequency dependence of the complex ratio $\tilde{i}/\tilde{\Omega}$ is given by the EHD impedance [11].

For 0.5 and 0.1 M NaCl (Figs 4 and 5), the phase shift and reduced amplitude of $\tilde{i}/\tilde{\Omega}$ obtained without ohmic drop compensation at two different Ω values (25.1 and 125.7 rad s^{-1}) merge reasonably well on a single curve at each concentration for values of reduced frequency $p = \omega/\bar{\Omega}$ lower than 0.3. This behaviour is characteristic of a process totally controlled by mass transport to a uniformly accessible interface for which the theory predicts that the data are function of a single dimensionless frequency $pSc^{1/3}$ [15]. The Schmidt number Sc is characteristic of the diffusing species in the solution and is defined as the ratio of the kinematic viscosity, ν, to the diffusivity, D [13].

For $p > 0.3$, the experimental data show a systematic deviation, especially on the phase shift from

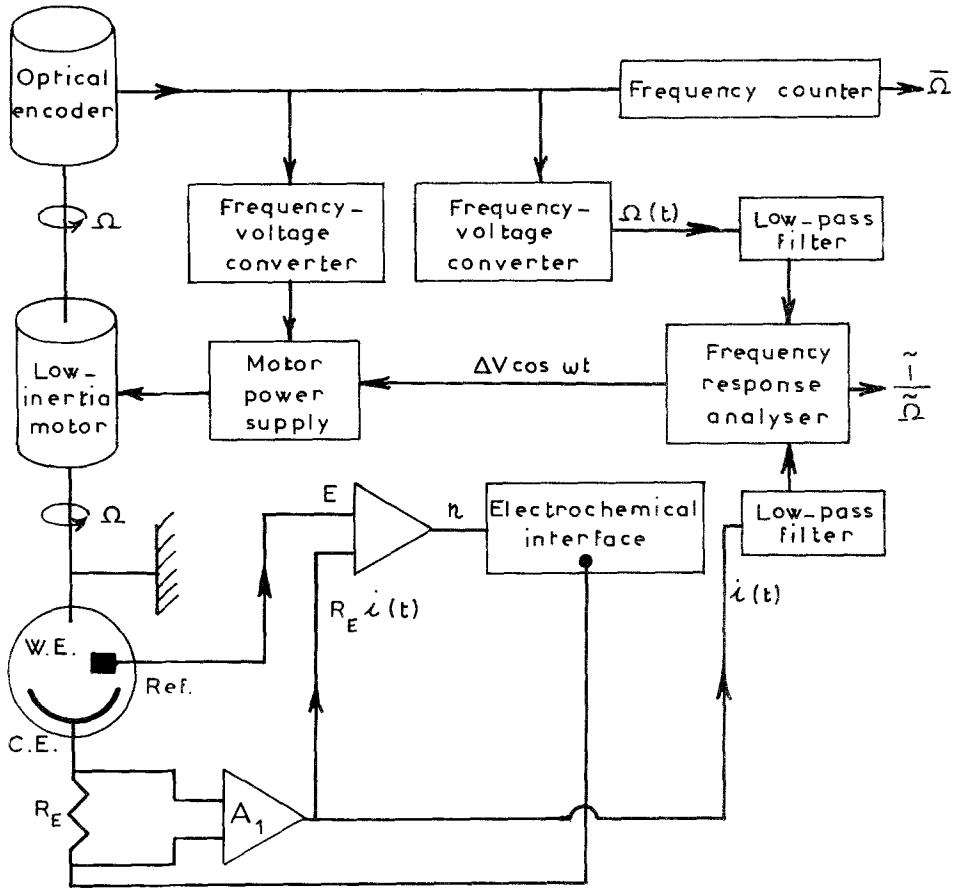

Fig. 1. Experimental setup. WE, Ref. and CE are the working, reference and counter electrodes, respectively. The current is measured at output of A_1. The overpotential is regulated by using ohmic drop compensation.

the theoretical asymptotic value of 180° [15]. Also, the experimental values separate from one another and no longer lie on a single curve.

For a 0.02 M NaCl solution, the data obtained without ohmic drop compensation at two different mean velocities (25.1 and 125.7 rad s^{-1}) do not merge on a single curve for phase shift or amplitude dependence whatever the p value. When automatic ohmic drop compensation is used (the electrolyte resistance is 547 ohms), the data fall again on a single curve at low p values (Fig. 6), with the same deviation at high p values as that displayed in Figs 4 and 5.

For a 0.0033 M NaCl solution, the automatic ohmic drop compensation of 3 320 ohms (the resistance of the electrolyte is 3 445 ohms) reduces the divergence between the two curves but does not succeed in merging the data onto a single curve (Fig. 7).

All this data cannot be analysed by considering that mass transport is the rate determining process. A quantitative treatment taking into account the finite electron transfer rate was developed and used for determining Sc.

4. Discussion

The function $H(\omega)$ in Equation 2 can be defined as the response of the diffusion current to a sine wave modulation of the wall velocity gradient. This function is thus the equivalent for a microelectrode to the EHD impedance $\tilde{i}/\tilde{\Omega}$ for the RDE. Indeed, for ideal mass transport control at a RDE, the expression is

$$\left(\frac{\tilde{i}}{\tilde{\Omega}}\right) = \left(\frac{\bar{i}}{\bar{\Omega}}\right) W_0 \tag{7}$$

where W_0 is tabulated in [15].

A similar equation can then be obtained for $H(\omega)$

$$\left(\frac{\tilde{i}}{\tilde{\alpha}}\right) = \frac{1}{3}\left(\frac{\bar{i}}{\bar{\alpha}}\right) H(\omega) \tag{8}$$

where $H(\omega)$ has been calculated in [16] for circular or rectangular microelectrodes.

In this work, analogs of Equations 7 and 8 were calculated by considering nonideal mass transport control. Most of the calculations are presented for a RDE and the corresponding result for a microelectrode is readily deduced.

Let us first represent the behaviour of the metal/electrolyte interface as an equivalent electrical circuit (Fig. 8). In this scheme, all electrical quantities in the frequency domain bear a tilde mark (~). The only assumption is the separation into a faradaic branch which is associated with electron transfer, and a capacitive branch due to the double layer effect. Hence, the total measured current, $\tilde{i}$, is defined as

$$\tilde{i} = \tilde{i}_F + j\omega C_D \tilde{\eta} \tag{9}$$

Since the potentials are referred to a reference electrode in solution, the potential drop is the sum

$$\tilde{E} = R_E \tilde{i} + \tilde{\eta} \tag{10}$$

where $\tilde{\eta}$ is the overpotential at the interface.

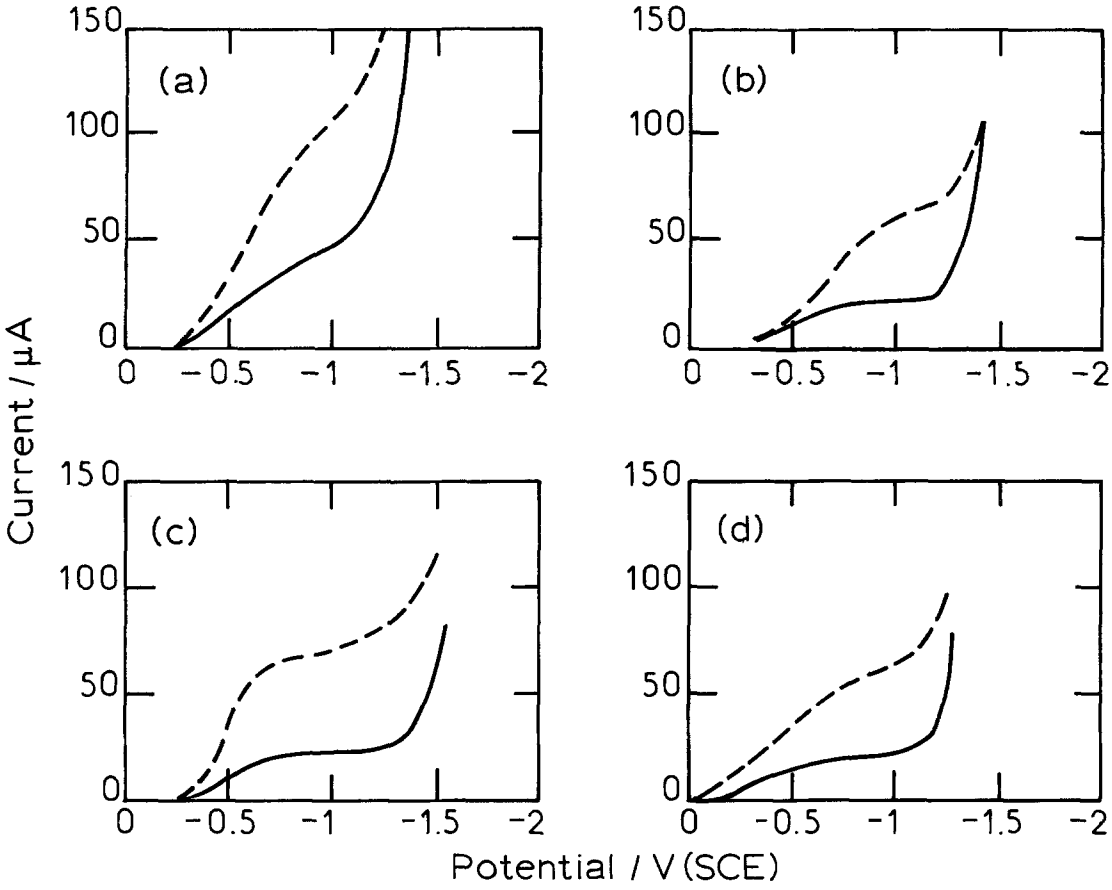

Fig. 2. Current–potential curves for oxygen reduction in NaCl solutions. NaCl concentration: (a) 0.5, (b) 0.1, (c) 0.02 and 0.0033 M. Curves at 0.02 M and at 0.0033 M have been plotted with an ohmic drop compensation.

Considering a significant overpotential due to the electrochemical reaction, a Tafel law for the faradaic current is assumed:

$$i_F = nFkc_0 \exp b\eta \qquad (11)$$

where n is the number of electrons exchanged (four in the case of oxygen), k is the rate constant and c_0 is the concentration of diffusing species at the wall.

For perturbation quantities the expression is

$$\frac{\tilde{i}_F}{nF} = k \exp(b\eta)\tilde{c}_0 + kc_0 b \exp(b\eta)\tilde{\eta} \qquad (12)$$

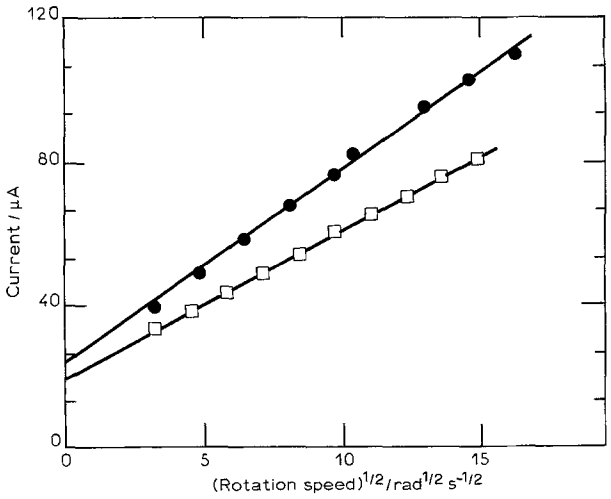

Fig. 3. Limiting current against $\Omega^{1/2}$ plots at $E = -1$ V/SCE. NaCl concentration: (●) 0.5 and (□)0.0033 M.

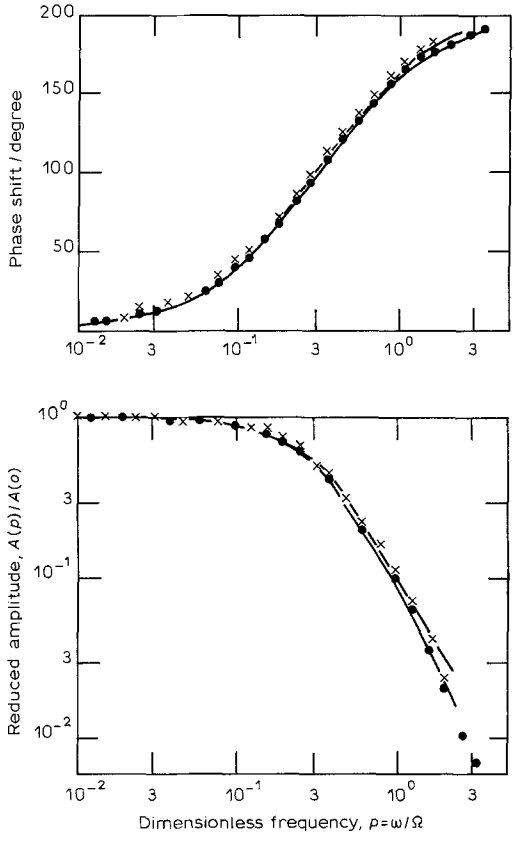

Fig. 4. EHD impedance diagrams for 0.5 M NaCl solution. The solid lines are Equation 17 fitted to the experimental data for: (●) $\Omega = 25.1$ and (×) 125.7 rad s^{-1}. See Table 1.

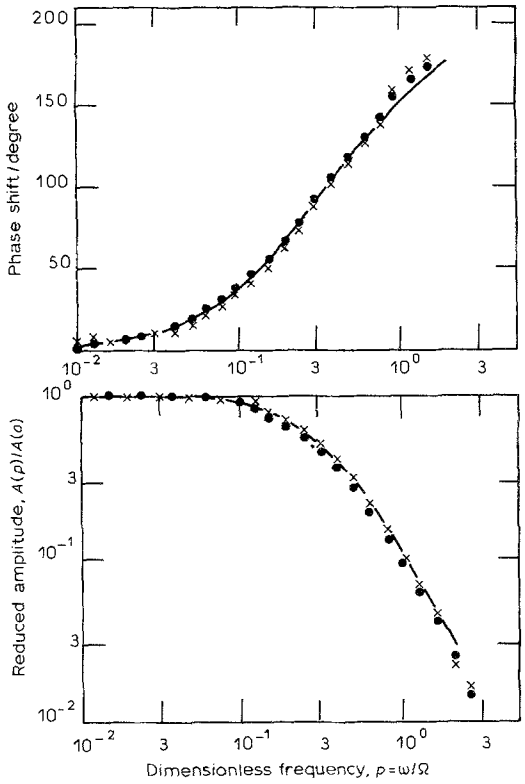

Fig. 5. EHD impedance diagrams for 0.1 M NaCl solution. Symbols as for Fig. 4.

For the usual diffusion plateau conditions, c_0 and $\tilde{c}_0$ are negligibly small. Here they are assumed to be nonzero. This equation gives the impedance Z_F of the 'faradaic branch' as the sum of the charge transfer

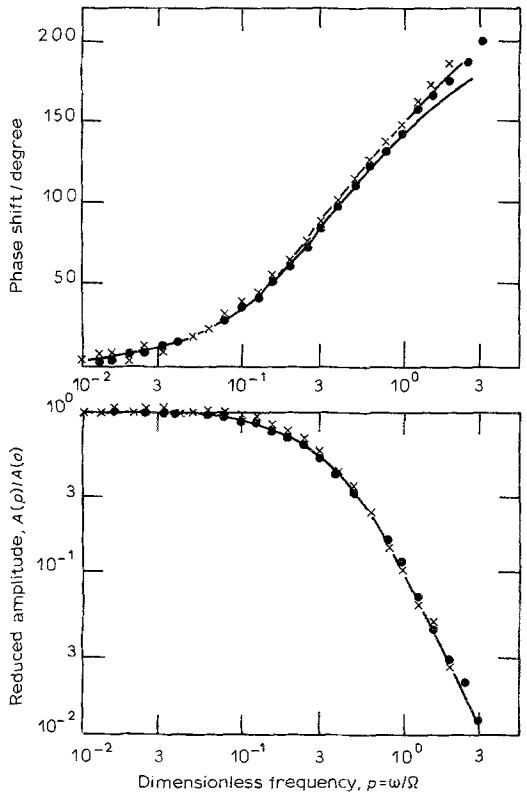

Fig. 6. EHD impedance diagrams for 0.02 M NaCl solution. Measurements have been done with an ohmic drop compensation. Symbols as for Fig. 4.

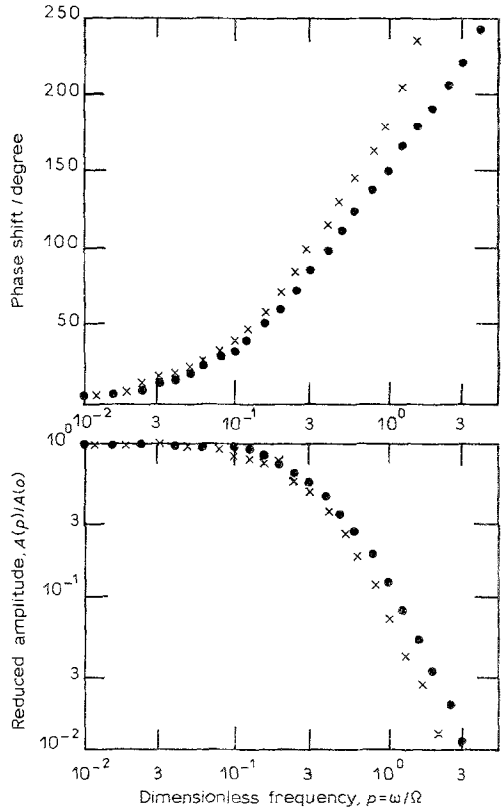

Fig. 7. EHD impedance diagrams for 0.0033 M NaCl solution. Measurements have been done with an ohmic drop compensation. Symbols as for Fig. 4.

resistance R_t and the diffusion impedance Z_D (see Fig. 8) where

$$R_t^{-1} = nFkc_0 b \exp(b\eta) \tag{13a}$$

$$Z_D = -nFc_0 bD\theta_0'/\delta \tag{13b}$$

Here, $\delta = 1.61D^{1/3}\nu^{1/6}\Omega^{-1/2}$ is the thickness of the Nernst layer and $-1/\theta_0'$ is the dimensionless convective Warburg impedance, which is a function of $pSc^{1/3}$ only [15].

At the interface, the flux conservation is

$$\frac{\tilde{i}_F}{nF} = D\left.\frac{\partial\tilde{c}}{\partial y}\right|_0 \tag{14}$$

and the relation between flux and concentration [15] is

$$\left.\frac{\partial\tilde{c}}{\partial y}\right|_0 = -\frac{\tilde{c}_0}{\delta}\theta_0' + \frac{\tilde{\Omega}}{\Omega}\left.\frac{\partial\tilde{c}}{\partial y}\right|_0 W_0 \tag{15}$$

where W_0 is defined in Equation 7. Of the unknowns

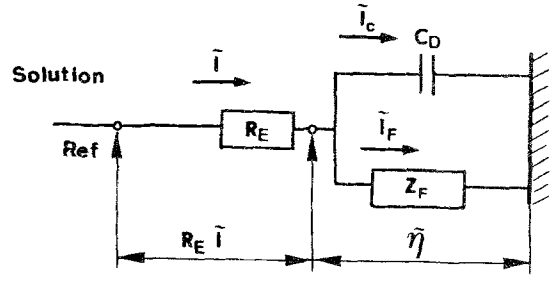

Fig. 8. Electrical equivalent circuit of the interface. R_E is the electrolyte resistance, C_D is the double layer capacitance, and Z_F is the faradaic impedance which is the sum of the charge transfer resistance R_t and the diffusion impedance Z_D.

Table 1. Result of a nonlinear fitting of Equation 17 to experiments, determining Sc and i_l/i_k. The oxygen diffusivity and solubility are deduced by comparison of Equation 20 with steady-state data for each NaCl concentration

NaCl/M	$\Omega = 25.1\,rad\,s^{-1}$		$\Omega = 125.7\,rad\,s^{-1}$		$D \times 10^{-5}/cm^2\,s^{-1}$	$[O_2] \times 10^{-7}/mol\,cm^{-3}$
	Sc	i_l/i_k	Sc	i_l/i_k		
0.5	515	0.23	500	0.26	1.74	2.75
0.1	620	0.20	540	0.16	1.65	2.32
0.02	555	0.088	545	0.135	1.62	2.32

$\tilde{i}$, $\tilde{E}$, $\tilde{\Omega}$, $\tilde{c}_0$, $\tilde{\eta}$, $(\partial\tilde{c}/\partial y)|_0$ and $\tilde{i}_F$, the non observable quantities $\tilde{c}_0$, $\tilde{\eta}$, $(\partial\tilde{c}/\partial y)|_0$ and $\tilde{i}_F$ can be eliminated by use of Equations 9, 10, 12, 14 and 15, to obtain a relation between observable quantities $\tilde{i}$, $\tilde{E}$ and $\tilde{\Omega}$:

$$[R_E + (R_t + Z_D)(1 + j\omega R_E C_D)]\tilde{i} - [1 + (R_t + Z_D)j\omega C_D]\tilde{E} = \left(\frac{\bar{i}}{\bar{\Omega}}\right) Z_D W_0 \tilde{\Omega} \tag{16}$$

By use of potentiostatic regulation ($\tilde{E} = 0$):

$$\left(\frac{\tilde{i}}{\tilde{\Omega}}\right) = \left(\frac{\bar{i}}{\bar{\Omega}}\right) \frac{Z_D}{R_E + (R_t + Z_D)(1 + j\omega R_E C_D)} W_0 \tag{17}$$

When $R_E = 0$, a situation realized either by using a larger excess of supporting electrolyte (i.e. at 0.5 or even 0.1 M NaCl) or by using ohmic drop compensation, the same result is obtained by directly writing $\tilde{i} = \tilde{i}_F$, because there is no modulation of the interfacial potential. However, there is no proportionality between $\tilde{i}/\tilde{\Omega}$ and W_0, because of the factor $Z_D/(R_t + Z_D)$.

For a very fast electrochemical reaction on the diffusion plateau, $R_t \ll |Z_D|$, even at mid-frequencies, so that $Z_D/(R_t + Z_D) = 1$, and $(\tilde{i}/\tilde{\Omega}) = (\bar{i}/\bar{\Omega})W_0$. More generally from Equation 13,

$$\frac{Z_D}{R_t + Z_D} = \frac{1}{1 + (i_l/i_k)(-\theta_0')} \tag{18}$$

where

$$i_k = nFc_\infty k \exp b\eta \tag{19}$$

is the kinetic current at the same potential which would be observed if mass transport were not rate determining. Since $(-\theta_0')$ in Equation 18 depends only on $pSc^{1/3}$, Equation 17 with $R_E = 0$ depends only on two parameters: *Sc* and i_l/i_k.

The curves in Figs 4–7 have been obtained by a nonlinear least-square fit, adjusting *Sc* and i_l/i_k in Equation 17. The results of the fitting procedure are shown in Table 1. The *Sc* values are only slightly dependent on chloride concentration, except for the value at 0.1 M for 25.1 rad s^{-1}.

For 0.02 M, the ratio i_l/i_k varies approximately as $\Omega^{1/2}$ as expected.

The kinematic viscosity ν is almost independent of NaCl concentration between 0.5 and 0.02 M. Using $\nu = 0.89 \times 10^{-2}\,cm^2\,s^{-1}$, at 25° C as a mean, gives the values of *D* reported in Table 1. These values are 13 to 20% below those obtained from a correlation in [14] and established from more than 25 sources based on various experimental techniques. The EHD technique under best conditions (i.e. ideal diffusion plateau) has an uncertainty of 5% [17]. Since two parameters were simultaneously adjusted, the uncertainty of the fitted values is increased to approximately 10 to 15%.

The oxygen solubilities in Table 1 were obtained by fitting

$$i = \frac{i_l}{1 + i_l/i_k} \tag{20}$$

to the steady-state current. This corresponds to the factor in Equation 18. The results agree reasonably well with [18] and [19], the latter reporting values for the solubility between 2.1 and 2.5 $\times 10^{-4}$ M in the chloride concentration investigated.

4.1. *Proton reduction*

Though the current due to proton reduction is not diffusion controlled and is in parallel to the current due to the oxygen reduction, it is necessary to evaluate the relevant effect on the EHD impedance. A faradaic branch in parallel to that corresponding to oxygen reduction must then be added to the equivalent circuit of Fig. 8. Equation 9 then becomes

$$\tilde{i} = \tilde{i}_{F1} + \tilde{i}_{F2} + j\omega C_D \tilde{\eta} \tag{21}$$

where $\tilde{i}_{F1}$ stands for oxygen reduction and $\tilde{i}_{F2}$ for proton reduction.

By assuming that in this potential range, Z_{F2} does not contain a diffusion impedance and by ascribing subscripts 1 in Equation 14, then

$$\left(\frac{\tilde{i}}{\tilde{\Omega}}\right) = \left(\frac{\bar{i}_{F1}}{\bar{\Omega}}\right) \times \frac{Z_{D1}}{R_E + [1 + j\omega R_E C_D + R_E Z_{F2}^{-1}](R_{t1} + Z_{D1})} W_0 \tag{22}$$

Hence, the parallel reaction increases the real part of the expression between brackets without changing the imaginary part, and so reduces the phase increase, which is good. On the other hand, the amplitude is divided by the coefficient $1 + R_E Z_{F2}^{-1}$, which is undesirable for spectrum analysis. When R_E is compensated, Equation 22 reduces to Equation 17 with $R_E = 0$ and the problem disappears. Without compensation for R_E, the consideration of the product $R_E C_D$ in the fitting procedure was probably not enough for the 0.5 or 0.1 M solutions, and the influence of the faradaic branch due to hydrogen evolution

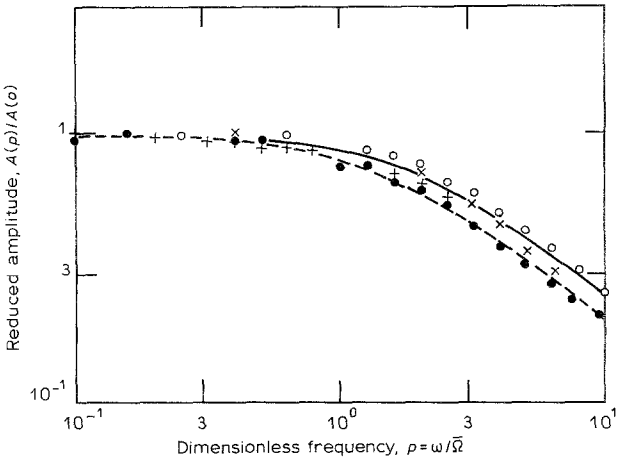

Fig. 9. Amplitude of the EHD impedance against $p = \omega/\Omega$ for a microelectrode embedded in the disc plane. Diameter 0.5 mm and distance from the rotation axis 5 mm. Oxygen reduction (×) 60 r.p.m.; (○) 120 r.p.m.; (+) 240 r.p.m. (——) Theoretical response of $H(\omega)$ with $Sc = 500$; ferricyanide reduction (●) 240 r.p.m.; (– – – –) theoretical response of $H(\omega)$ with $Sc = 1150$.

would be significant, presumably because, in this instance, this faradaic impedance is not reducible to a simple charge transfer resistance.

4.2. *Application to a microelectrode*

In Equations 9 to 16 the only modifications are as follows. The expression $-1/\theta_0'$ in Equation 15 now represents the dimensionless convective Warburg impedance of a microelectrode [20]. Also Equation 15 becomes

$$\left.\frac{\partial \tilde{c}}{\partial y}\right|_0 = -\frac{\theta_0'}{\delta}\tilde{c}_0 + \frac{1}{3}\left(\left.\frac{\partial \bar{c}}{\partial y}\right|_0 \Big/ \bar{\alpha}\right) H(\omega)\tilde{\alpha} \quad (23)$$

Then, Equation 17 becomes

$$\left(\frac{\tilde{i}}{\tilde{\alpha}}\right) = \frac{1}{3}\left(\frac{\bar{i}}{\bar{\alpha}}\right)\frac{Z_D}{R_E + (R_t + Z_d)[1 + j\omega R_E C_D]} H(\omega) \quad (24)$$

As a consequence of Equation 24, a correct use of Equation 2 requires that $H(\omega)$ is replaced by $Z_D/R_E + [1 + j\omega R_E C_D](R_t + Z_D)H(\omega)$.

In the case of a microelectrode, the effect of ohmic drop is less important since R_E varies as d^{-1} (d = microelectrode diameter) and C_D varies as d^2, so the product $R_E C_D$ varies as d and plays a smaller role. In contrast with the RDE case, the effect of $Z_D/(R_t + Z_D)$ can be more important since the mass transport rate is increased, and therefore R_t is increased with respect to Z_D.

In order to be closer to the actual conditions of use, measurement of the dynamic response $H(\omega)$ of a microelectrode with oxygen reduction was directly performed by embedding a circular microelectrode in an insulating disc electrode. The theory and experimental verification for this flow geometry was presented in [16].

The response observed with a fast redox system, the ferri-ferrocyanide couple in KCl[M], was compared to that due to the oxygen reduction. As can be observed in Fig. 9, the dependence of amplitude on dimensionless frequency is the same for the oxygen reduction (○, ×, +) and the ferricyanide reduction (●, – – – –). The frequency shift between the two systems is only due to the difference in the Schmidt number values for the two species, i.e. $Sc(O_2) \sim 500$ and $Sc(\text{ferri}) \sim 1150$ [17]. As a slight deviation is noticed when varying Ω, the results show that the oxygen reduction is appropriate for power spectral density measurements, but accurate analysis would require the correction given by Equation 24.

5. Conclusion

The work presented demonstrates the possibility of using the oxygen reduction as tracer reaction for measurements of fluctuating hydrodynamic quantities. Ordinary fresh water can be used satisfactorily as the electrolyte. One problem likely to arise is the presence of significant amounts of carbonates which can precipitate and form a scale deposit because of the pH increase induced by the oxygen reduction. Scale inhibitors, acting at very low concentrations, can be used in this instance. Also, a local acidity increase can be imposed by a temporary anodic polarization.

The necessity of removing the ohmic drop at low conductivities requires another experimental difficulty to be overcome. In hydrodynamic applications of polarography, regulation devices of the current-follower type involving two electrodes are generally used [21]. When using oxygen reduction, this type of regulation is not recommended for two reasons. First, (i) the ohmic drop cannot be correctly compensated. Secondly, (ii) the counter electrode must have a large area with respect to that of the working electrode, and, with no foreign ions added to the water, the counter electrode behaves as a quasi ideally polarizable electrode. Therefore, when the fluid velocity fluctuates, the current on the working electrode also fluctuates, and so the potential of the counter electrode which is used as reference. This, in turn, modifies the current on the working electrode. Those drawbacks can be avoided by using a potentiostat.

Acknowledgements

This work was supported in part by the NATO grant OTAN 86/0774 for international collaboration in research.

References

[1] M. A. Leveque, *Ann. Mines* **13** (1928) 283.
[2] R. D. Patel, J. J. McFeely and K. J. Jolls, *AIChE J.* **21** (1975) 259.
[3] C. Deslouis, B. Tribollet and L. Viet, 4th International Conference on Physicochemical Hydrodynamics, *Ann. NY Acad. Sci.* **404** (1983) 471.
[4] V. E. Nakoryakov, A. P. Budukov, O. N. Kashinsky and P. I. Geshev, IUTAM Symposium, Nancy, France, 695–721 (1983).
[5] G. Vlachos, *Ann. I.T.B.T.P.* **468** (1988) 70–91.
[6] A. Caprani, C. Deslouis, I. Epelboin and B. Tribollet, *Bioelectrochemistry and Bioenergetics* **2** (1975) 351.
[7] J. Pauli, M. Henlsher and U. Onken, 10th International Congress of Chemical Engineering, 'CHISA 90', Prague

(1990).
[8] J. Lelievre, Cl. LeFeuvre and R. Gaboriaud, *C.R. Acad. Sci. Ser. C* **275** (1972) 1455.
[9] J. P. Hoare, 'The Electrochemistry of Oxygen', Interscience Publishers, Wiley & Sons, New York (1968).
[10] B. T. Ellison and I. Cornet, *J. Electrochem. Soc.* **118** (1971) 68–72.
[11] C. Deslouis, C. Gabrielli, Ph. Sainte-Rose Fanchine and B. Tribollet, *J. Electrochem. Soc.* **129** (1982) 107.
[12] Y. Okinaka, R. Sard, C. Wolowodiuk, W. H. Craft and T. F. Retajczyk. *J. Electrochem. Soc.* **121** (1974) 56.
[13] V. G. Levich, 'Physicochemical Hydrodynamics', Prentice-Hall, Englewood Cliffs, NJ (1962).
[14] C. E. Saint-Denis and C. J. D. Fell, *Can. J. Ch. Eng.* **49** (1971) 855.
[15] B. Tribollet and J. Newman, *J. Electrochem. Soc.* **130** (1983) 2016.
[16] C. Deslouis, O. Gil and B. Tribollet, *J. Fluid Mech.* **215** (1990) 85–100.
[17] B. Robertson, B. Tribollet and C. Deslouis, *J. Electrochem. Soc.* **135** (1988) 2279.
[18] G. W. C. Kaye and T. H. Laby, 'Tables of Physical and chemical constants', 14th ed. Longman, London (1973).
[19] M. L. Hitchman, 'Measurement of dissolved oxygen', in 'Chemical Analysis', a series of monographs on analytical chemistry and its applications, Vol 49 (edited by P. J. Elving and J. D. Winefordner), John Wiley & Sons, New York (1978).
[20] C. Deslouis, B. Tribollet and M. A. Vorotyntsev, *J. Electrochem. Soc.* **138** (1991) 2651.
[21] T. J. Hanratty and J. A. Campbell, in 'Fluid Mechanics Measurements', (edited by R. J. Goldstein), Hemisphere, Washington DC (1983).